Original article

JOURNAL OF REINFORCED PLASTICS & COMPOSITES

Journal of Reinforced Plastics and Composites
2018, Vol. 37(10) 716–727

DOI: 10.1177/0731684418761224
journals.sagepub.com/home/jrp
SAGE

Polyvinyl alcohol reinforced with carbon nanotubes for fused deposition modeling

D Rigotti, L Fambri and A Pegoretti

Abstract

For the first time, nanocomposite filaments consisting of polyvinyl alcohol and carbon nanotubes were successfully used for additive manufacturing by fused deposition modeling. Polyvinyl alcohol and carbon nanotubes were mixed in a water solution using hexadecyl trimethyl ammonium bromide as a surfactant. Filaments with various concentrations of carbon nanotubes (up to a maximum content of 3 wt.%) were obtained with a single screw extruder and used to feed a commercial desktop 3D printer. Carbon nanotubes increase the glass transition temperature of the printed samples; however, the presence of CTAB reduces this effect. The viscosity of the material increases with the addition of carbon nanotubes and the 3D-printed samples become tougher as the carbon nanotubes amount increases. Elastic modulus and creep compliance are remarkably improved by the presence of carbon nanotubes, while ultimate mechanical properties are not affected. The high reduction of electrical resistivity found on the filaments was not found on the 3D-printed samples. This was attributed to the prevalent location of carbon nanotubes in the core region of the 3D-printed samples as documented by scanning electron microscopy.

Keywords

Additive manufacturing, fused deposition modeling, nanocomposites, carbon nanotubes

Introduction

Fused deposition modeling (FDM) or fused filament fabrication (FFF) is one of the fastest spreading technology among additive manufacturing (AM) techniques due to the continuous decrease of the related costs. FDM is a technique to build up objects layer-by-layer with the support of computer aided design. The strong points of FDM over traditional manufacturing are the possibility of free design and no need to use mold in manufacturing, thus allowing the realization of complex parts. A 3D model of an object is first converted to a stereo lithographic (STL) format. By using a specific software, the STL file is sliced in layers before to be sent as a G-code to the 3D printing machine. A heated nozzle, mounted on a moving system, extrudes a thermoplastic polymer filament on a heated plate. According to the previously written G-code, the polymeric material is deposited in a controlled manner from the bottom layer to the top layer to form the final object. The development of new smart materials, nanocomposites and biomaterials could boost the growth of this AM technology.[1]

Polyvinyl alcohol (PVA) is known to be one of the few polymers soluble in water and susceptible of biodegradation in the presence of acclimated microorganisms.[2] PVA can be used in a broad field of applications, but it shows a high tendency to water sorption due to its hydrophilicity. This feature may impair its mechanical performances thus limiting its use for some intended applications.[3]

It is more than two decades that carbon nanotubes (CNTs) are recognized as one of the most promising reinforcing agents for polymers.[4] CNTs are known as one of the stiffest man made material, moreover their outstanding electrical and thermal conductivities generated a lot of interest for the production of CNT-reinforced nanocomposite materials with enhanced properties.[5] Dispersion of CNTs in a polymer matrix is a crucial aspect to obtain an effective reinforcing of

Department of Industrial Engineering, University of Trento, Trento, Italy

Corresponding author:
A Pegoretti, University of Trento, Via Sommarive 9, Trento 38123, Italy.
Email: alessandro.pegoretti@unitn.it

the final composite and a homogeneous dispersion of them inside the material is needed to maximize the performances.[6]

Different strategies to reach a good dispersion of CNTs in PVA were developed. One of the easiest method to prepare PVA/CNTs composites is through a mechanical way, simply stirring a water solution of PVA together with one containing CNTs. Chen et al.[7] dissolved PVA in water at 90°C to obtain a solution of 20 g of PVA per liter and used high power sonication (900 W) followed by a mild sonification to disperse CNTs at 1 wt.% in water. At the end, they were able to obtain films by solution casting with improved stiffness, strength and toughness over the neat polymer. Coleman et al.[8] prepared PVA/CNTs films with the same procedure to study the stiffening effect of the nanotubes in the matrix and to discern this effect from the increase in crystallinity at the matrix/filler interface. Double-walled CNTs and multi-walled CNTs were dispersed through ultrasonication in PVA by Ryan et al.,[9] who found an upper limit on CNTs concentration before aggregation (at about 1 wt.% of CNTs) below which the elastic modulus is expected to increase linearly with the filler content. A linear trend was also found by Wang et al.[10] for single-walled CNTs. Through different freeze/thaw cycles, PVA can be obtained in the form of hydrogel and CNTs are able again to effectively improve the mechanical properties of the PVA hydrogel.[11] PVA itself can enhance the dispersion of CNT in water-based solution limiting the need of chemical modification. Tsai and Huang[12] exploited this characteristic to produce biosensors for electrochemical application based on glassy carbon electrodes modified with PVA/CNT nanocomposite film. These electrodes manifested hydrophilicity and an excellent capacitive performance with good electrochemical stability.[13]

The use of surfactants to disperse hydrophobic filler in water could be a winning strategy to improve the mechanical and electrical properties of the composites. Castell et al.[14] studied the effect of combining different types of surfactants with polymer dispersants obtaining an increase of 12°C of the glass transition temperature at 2 wt.% of CNTs in PVA when sodium dodecylbenzenesulfonate (SDBS) and polyvinyl pyrrolidone (PVP) were used together. Various solutions for the dispersion of CNTs in water to obtain PVA/CNT composite can be found in the literature, one example is the use of Chinese ink as studied by Yan et al.[15] Ni et al.[16] improved the dispersion of CNTs in water using Arabic gum before mechanically mixing the suspension with the PVA solution.

In FDM technology, PVA found the main commercial application as vanishing support material for overhanging parts due to its particular feature to be hydro soluble so that it can be removed easily from the main object without any machining process. Hydrophilicity and hydro solubility of PVA triggered also increased interest in the biomedical field. PVA/hydroxyapatite scaffolds made with FDM technology exhibited a suitable porosity for promoting osteo-conduction and osteo-integration as reported by Cox et al.[17] In the last few years, the research on PVA in 3D printing was mainly focused on pharmacology application due to the possibility of producing 3D structures with tailored geometries and density, and thus the release concentration profile can be tuned carefully.[18,19] In this way, the introduction of 3D printing for drug delivery could be a revolution for customizable dosage drug-delivering devices.[20]

The incorporation of conductive nanofillers in polymers used in 3D printing is driven by the attempts to develop materials with tunable properties including elasticity, durability, water wettability and conductivity.[21] Even though a lot of work has been done in producing and studying different types of nanocomposite materials based on CNTs for FDM technology and different polymer matrices such as polylactide acid,[21] acrylonitrile butadiene styrene (ABS),[22] poly ether ether ketone (PEEK),[23] thermoplastic polyurethane (TPU),[24,25] polybutylene terephthalate (PBT),[26] to the best of our knowledge, no previous research addressing the fabrication of objects made by PVA/CNT through 3D printing FDM technologies is available in the open scientific literature.

Therefore, the present work is focused on the use of multi-walled CNTs to develop CNT/PVA composite filaments suitable to be printed with a desktop 3D printer. Furthermore, the effect of a surfactant to improve the dispersion of CNTs was investigated. A thermo-mechanical characterization of 3D-printed dumbbell specimen is also presented. Interest was focused on studying the effect of the increasing concentration of CNTs, the presence of surfactant and the different infill orientations.

Materials and methods

Materials

PVA was provided by Kuraray Specialties Europe GmbH (Frankfurt, Germany) under the trade name *Mowiflex TC 232*. Melt flow index (MFI) was 39±8 g/10 min a 190 °C under a constant load of 21.6 kg and the bulk density was 0.6–0.9 g/cm^3 according to the datasheet. Multi-walled carbon nanotubes (MWCNTs) were provided by Nanocyl SA (Sambreville, Belgium) with the trade name of *Nanocyl NC7000^{TM}*. They were produced via catalytic chemical vapor deposition (CCVD) and supplied as a

dry powder. The manufacturer datasheet reported an average diameter of 9.5 nm and a length of 1.5 μm, a surface area of 250–300 m^2/g (according to BET analysis) and a volume resistivity of 10^{-4} Ω cm. Hexadecyl trimethyl ammonium bromide (CTAB) was provided by Acros Organics and used as cationic surfactant for the dispersion of CNTs.

Preparation of 3D printable filaments

A solution of PVA and pure water (10% wt./wt.) was obtained immersing the PVA granules in water under stirring for 2 h in a thermostatic bath at the temperature of 80°C. The addition of CNTs was performed in two different ways, depending on the presence or not of CTAB. When no surfactant was used, CNTs were directly added to the PVA solution and magnetically stirred for 2 h. After this time, the PVA/CNTs solution was sonicated for 5 min with a power of 200 W with a Hielscher 400S ultra-sonicator equipped with a sonotrode of a 3 mm diameter. After the sonication, the solution was stirred for 1 h and cooled down.

On the other hand, when CTAB was used, a solution of pure water with 1% w/w of CNTs and 0.1% w/w of CTAB was prepared. This solution was stirred at room temperature for 2 h and then sonicated with the same equipment used before. After the sonication, the solution was added to the PVA one and it was stirred for 1 h. All the formulations were then degassed with a vacuum pump until the complete bubbles removal was reached. Finally, the solutions were casted in silicon molds and dried in an oven at 60°C for 72 h to obtain plates of both neat PVA and PVA/CNT.

These plates were cut into small pieces and they were put into a refrigerator at −20°C to cool the material under the glass transition temperature before grinding. The obtained powders were kept in an oven at 70°C under vacuum for four days to completely remove the humidity.

The extrusion was performed with a single screw extruder (Estru 13, Friul Filiere SpA, Udine, Italy) with a screw diameter of 14 mm and an extrusion die with a head of 3.0 mm. The temperature profile of the extruder was 125°C for the feeding head and 175°C for the final extrusion die. Filaments with a diameter of 1.75 mm and different concentration in CNTs, suitable for the following FDM process, were successfully extruded.

3D printing by FDM. A digital 3D model of the dumbbell specimens according to ISO527 standard was built with the aid of the software SolidWorks® and it was exported in STL format. Through the freeware software Slic3r, a G-code file was compiled with the following parameters for the printing: rectilinear type of infill, infill percentage 100%, no raft, layer height 0.2 mm, nozzle temperature 230°C, bed temperature 40°C deposition rate 40 mm/s. Different infill angles were studied 0°, ±45° and 0°–90°. The 3D printer used for the production of the samples was a Sharebot Next Generation desktop 3D printer provided by Sharebot NG with a nozzle diameter of 0.35 mm. Different kinds of samples with a rectangular shape for the measurement of the electrical resistivity were printed with printing directions along the y-axis and z-axis.

Testing techniques

Microstructural observations of cryo-fractured surfaces of the 3D-printed specimens were performed by a Zeiss Supra 40 high resolution field emission scanning electron microscope (FESEM) with an accelerating voltage of 2.5 kV, after a platinum palladium conductive coating of the samples.

Viscosity of the composite material was investigated by MFI tests according to ASTM 1238–04 standard. MFI tests were performed using a Kayeness 4003DE capillary rheometer at a temperature of 210°C and with a load of 2.16 kg. Before testing, the samples were kept under vacuum at 70°C for 72 h to remove completely the humidity.

Degradation at a constant heating rate was investigated by thermogravimetric analysis (TGA). The analysis was performed by a TGAQ500 (TA Instruments, USA), at a heating rate of 10°C/min (under N_2) in the range between 40°C and 700°C.

Differential scanning calorimetry (DSC) was performed by a Mettler DSC 30 calorimeter. Tests were performed from −10°C to 250°C at a heating and cooling rate of 10°C/min under a nitrogen flow of 150 ml/min. Glass transition temperature T_g, melting temperature T_m and the degree of crystallinity χ_c were evaluated. The value of enthalpy for fully crystalline PVA was taken equal to 161.4 J/g.[27]

The water sorption of the material was evaluated by controlling the change of weight of at least five samples for each composition during time. The samples were kept under vacuum at 50°C for two days to reach their complete drying and then stored into a container at 23°C with 55% of relative humidity. The value of the water sorption was measured, according to the ASTM D570 standard, by the change of weight of the samples.

Dynamic mechanical thermal analysis (DMTA) tests were carried out using a TA Instrument DMA Q800 device, in the temperature range −10°C to 150°C, with a heating rate of 3°C/min, a strain amplitude of 0.05% and a frequency of 1 Hz. Through this analysis, it was possible to evaluate the storage modulus (E′), the loss modulus (E″) and the loss tangent (tan δ) as a function of the temperature.

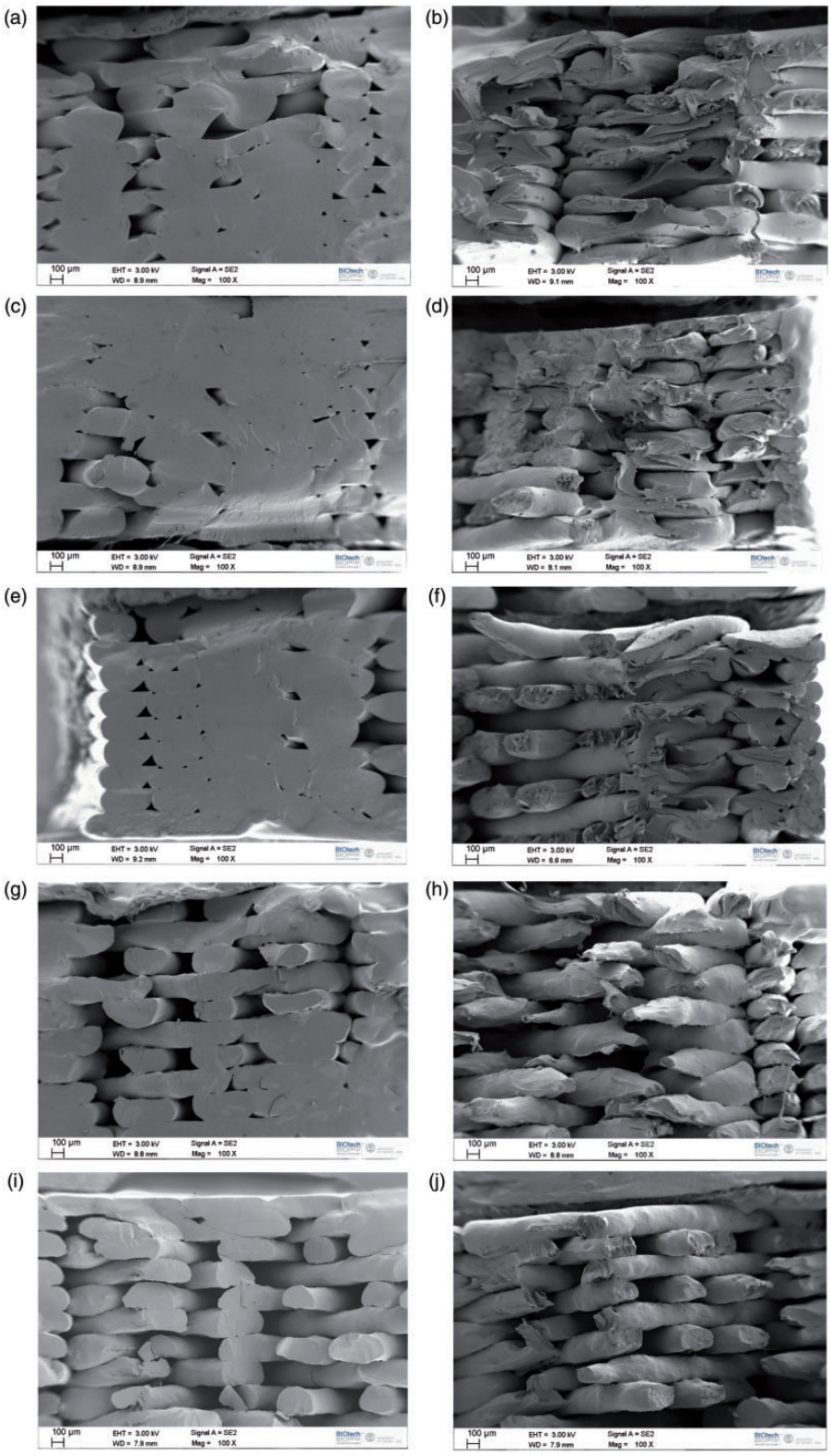

Figure 1. SEM micrographs of the 3D-printed samples: neat PVA (a–b), 1 wt.% of CNT (c–d), 1 wt.% of CNT and CTAB (e–f).

The creep test permitted to evaluate the effect of the nanofillers on the resistance to deformation under constant stress and temperature. The analysis was performed with a TA Instrument DMA Q800 with an applied stress of 1.75 MPa at a temperature of 30°C for a period of 60 min.

Quasi-static tensile tests allowed to collect data related to both the elastic behavior and the failure properties of the material. They were performed using an Instron 5969 elettromechanical testing machine, equipped with a 50 kN cell load, at room temperature with a crosshead speed of 100 mm/min. The deformation was measured with a long-travel extensometer Instron 2603 according to the standard ISO 527. At least five specimens for each composition were tested to estimate the average values of stress at break (σ_r) and elongation at break (ε_b).

The electrical volume resistivity was measured following the ASTM D4496 standard for moderately conductive materials with a Keithley 6517A. The resistivity has been measured using two points contact configuration at room temperature with an applied voltage of 0.1 V. The specimens were connected to the ohmmeter through two alligator clips on a gage length of 10 mm and the resistance was averaged over a testing period of 30 s.

Results and discussion

Microstructure

The microstructure of the 3D-printed parts is a key factor in the understanding of the quality of the FDM process and can reveal important details. In Figure 1, low-magnification FESEM pictures of the fracture surfaces after cryogenic fracture (Figure 1(a), (c), (e), (g) and (i)) and after tensile tests (Figure 1(b), (d), (f), (h), (j)) for all the composition are presented.

The micrographs reveal that inside the specimens, the deposited filaments appear as flattened circle in the section for the neat polymer and become more elliptical as the CNT content increases. This could be attributed due to the increase in viscosity induced by the CNTs that in turn make the printing process more difficult because less material passes through the nozzle. The above-mentioned increase in viscosity leads to an increase in the part porosity. In FDM, specimens can be obtained with the neat polymer and triangularly shaped cavities can be observed, whose density increases with the CNTs amount. In the cryogenic fractured surface of the 3D-printed specimen made by neat PVA, the contour of the filaments that form the object is hard to recognize but became more evident in the samples loaded with 1 wt.% of CNTs. At the highest concentration of CNTs (3 wt.%), filaments can be clearly distinguished inside the printed part and low adhesion between subsequent layers could be observed. The different microstructure of the 3D-printed samples, analyzed by the observation of the cryogenic fracture surface, can explain the different morphology of the fracture surfaces after tensile tests. The lower adhesion between layers leads to a higher deformation before the breaking of the filaments due to an enhancement of the mobility for rotations of single wires. The introduction of the surfactant with the CNTs seems to be detrimental for the quality of the 3D printing process, leading to a decrease in the adhesion between the filaments in comparison to the situation occurring without CTAB.

In Figure 2(a), a magnification of the sample loaded with 3 wt.% of CNTs is reported.

White areas are clearly visible inside the printed filaments and they correspond to CNTs aggregates. This non-homogenous distribution of CNTs inside the matrix could have a detrimental effect on the electrical properties of this material. In fact, the CNTs enriched

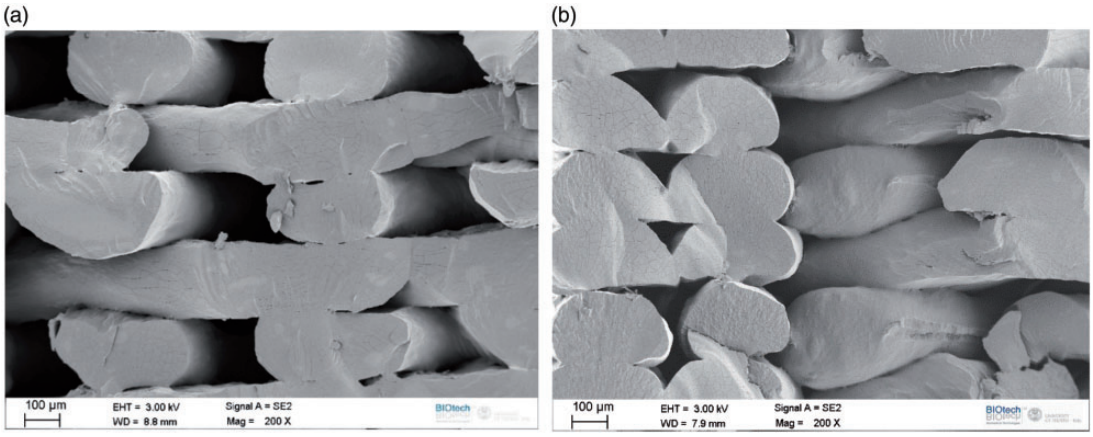

Figure 2. Magnification of samples loaded with 3 wt.% of CNTs without (a) and with surfactant (b).

areas are surrounded by neat PVA in the outer region near the filament surface. These CNTs rich areas are present also in the sample with CTAB but they appear to be smaller in size (Figure 2(b)). The adopted surfactant is therefore not able to promote a complete dispersion of CNTs inside the matrix.

Viscosity

Figure 3 summarizes the MFI values of neat PVA and relative nanocomposites when the CNTs content increases. The value of MFI decreases with the CNTs content, which corresponds to an increase of the viscosity of the system. The higher the quantity of nanotubes, the higher the viscosity of the system. At the same time, the presence of CTAB surfactant causes an increase in viscosity due to the better dispersion of CNTs in the matrix.

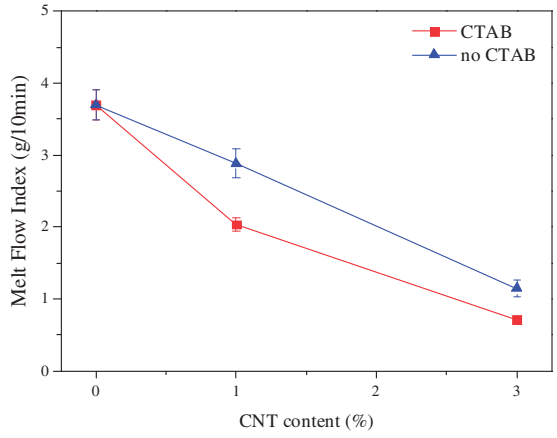

Figure 3. Melt flow index as a function of CNT content with and without surfactant.

Thermal analysis

TGA was performed to investigate the thermal behavior of the filaments of neat PVA and its nanocomposites inside the nozzle of the 3D printer, where higher temperature is needed to assure a good quality of the printed samples. In Figure 4, the TGA thermograms and the derivative curves of the mass loss are reported.

In Table 1, the values of the temperature when a mass loss of 5% is reached ($T_{5\%}$), that correspond to the onset of the degradation, the temperature at the maximum degradation rate (T_{max}) and the residual mass at 700°C are summarized.

The thermographs clearly show two degradation steps, according to the derivative curves (Figure 4(a)), that is typical of PVA. The first step corresponds to the release of water, and the second one to the evolution of volatiles.[28] The introduction of CNTs in the matrix affects the first degradation step, shifting the curves towards higher temperatures. This is a positive effect moving $T_{5\%}$ from 222°C of the neat polymer to 240°C, so the resistance to degradation of the PVA near the processing temperature is increased. The maximum

Table 1. Onset degradation temperature ($T_{5\%}$), temperature for maximum rate of degradation (T_{max}) and residual mass values from thermogravimetric analysis.

	$T_{5\%}$ (°C)	T_{max} (°C)	Residual mass at 700°C (%)
PVA_neat	222.2	343.8	0.4
PVA_CNT-01	240.8	344.7	4.4
PVA_CNT-01_CTAB	242.3	357.0	4.2
PVA_CNT-03	238.2	344.7	4.0
PVA_CNT-03_CTAB	241.9	355.3	6.2

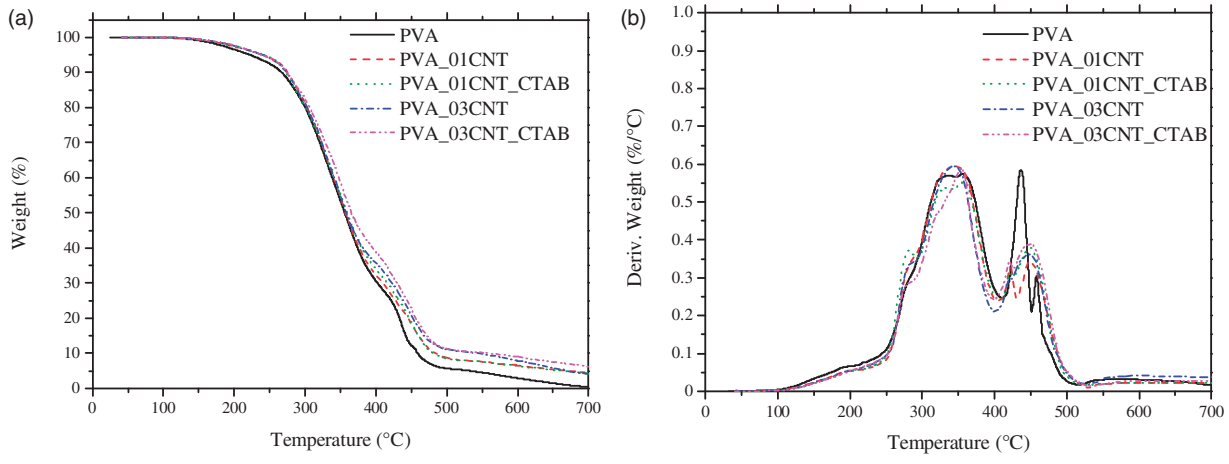

Figure 4. Thermogravimetric curves (a) and derivative curves (b) from TGA.

rate of degradation is located, according to the maximum of the derivative curve, at about 340°C for all the composition which is increased to about 10°C for the sample containing the surfactant maybe due to a better dispersion of CNTs inside the matrix. Residual mass at 700°C increased since CNTs do not suffer degradation in this temperature range.

Thermal properties of the 3D-printed samples were investigated using differential scanning calorimetry DSC. In Figure 5, calorimetry curves are shown for the heating (Figure 5(a)) and the cooling (Figure 5(b)) cycle, while Table 2 presents the transition temperature on heating (T_g), the melting temperature (T_m), the crystallization temperature on cooling (T_c) and the degree of crystallinity (X_c). CNTs and CTAB inside the matrix play opposite effects. In fact, CNTs induce an increase of the glass transition temperature but the presence of CTAB lowers this positive effect. It is possible to notice the same behavior in the values of T_m and T_c, where the temperatures are higher for the samples without surfactant. CNTs act as nucleating agents for the PVA and in fact the crystallization temperature during cooling slightly increases. Nevertheless, a slight decrease in the crystallinity content is measured when nanofillers are introduced in the matrix.

Water sorption

In Figure 6, the results of the test on the water absorption of the 3D-printed samples are reported. An almost constant humidity content is reached after seven days, with an increase of the 10% of the initial weight. The final quantity of absorbed water and the kinetic of absorption result are not to be affected by the incorporation of CNTs.

Mechanical properties

The effect of CNTs and CTAB addition on the viscoelastic properties at different temperature of the 3D-printed samples was evaluated through dynamic

Table 2. Glass transition temperature, melting temperature and crystallinity content for 3D-printed samples made of polyvinyl alcohol and relative nanocomposite from DSC results.

	T_g (°C)	T_m peak (°C)	T_c peak (°C)	χ_c (%)
PVA	37.4	176.7	134.4	14.3
PVA_01CNT	39.1	179.7	142.0	13.7
PVA_01CNT_CTAB	38.0	178.3	141.8	13.2
PVA_03CNT	48.1	181.3	143.1	12.1
PVA_03CNT_CTAB	38.7	179.2	141.8	13.1

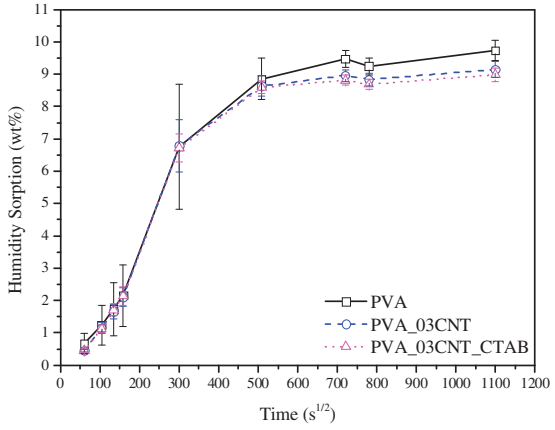

Figure 6. Humidity sorption of 3D-printed samples.

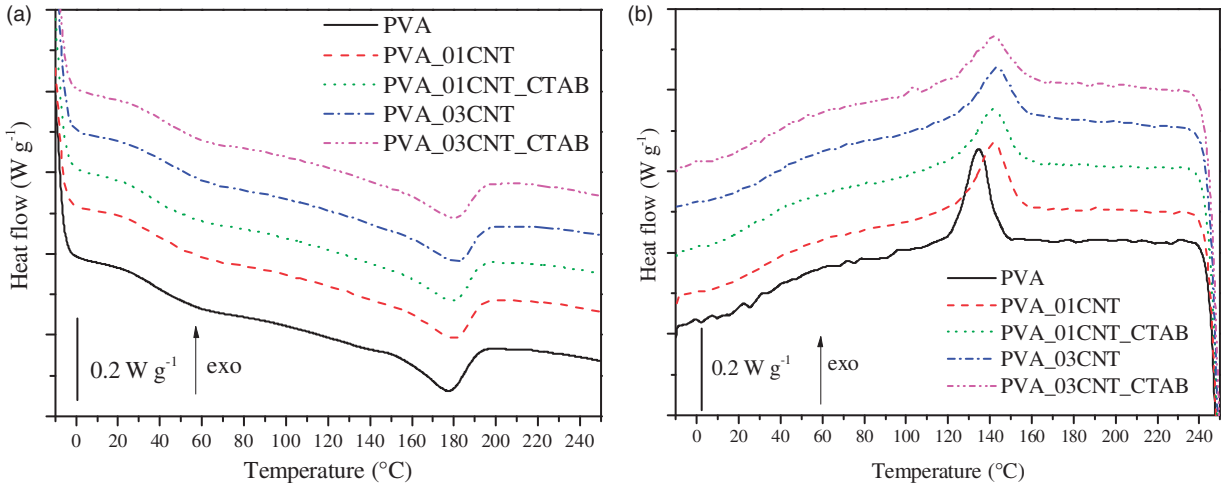

Figure 5. Differential scanning calorimetry curves on heating (a) and cooling (b) cycle for neat PVA and PVA/CNT composites. PVA: polyvinyl alcohol.

mechanical analysis on rectangular specimen printed at ±45° and their dynamic moduli and loss tangent values are shown in Figure 7, while the values of storage and loss moduli at 25°C and the peak of tanδ are reported in Table 3.

Storage and loss modulus appeared not to be influenced by the increasing content of nanotubes inside the matrix. Sample loaded with 3 wt.% of CNTs dispersed with the aid of CTAB showed the worse viscoelastic properties due to the increase in viscosity of the material and low printing quality as confirmed by the SEM observations. The damping absorption ability of the 3D-printed sample, corresponding to the value of tan δ peak, decreased with the increase of nanofiller as it is possible to notice from the value in Table 3 but CNTs increased the tanδ peak towards higher temperatures.

Tensile ultimate properties were evaluated for printed samples with different angle of infill and increasing amount of CNTs dispersed with or without the aid of the surfactant. The results are graphically summarized in Figure 8.

As expected, the best mechanical properties were found for the samples printed with the infill orientation angle of 0°/0° which manifests a stress at break value of 35.6 MPa in comparison of 28.4 MPa and 23.9 MPa

Table 3. Storage and loss modulus values at 25°C and location of the tan delta peak for printed samples of neat PVA and its nanocomposites.

	E′ at 25°C (GPa)	E″ at 25°C (MPa)	tanδ peak	tanδ peak (°C)
PVA	3.83	536.7	0.515	50.4
PVA_01CNT	3.81	507.7	0.456	50.9
PVA_01CNT_CTAB	4.00	522.1	0.458	50.6
PVA_03CNT	3.72	465.6	0.429	52.2
PVA_03CNT_CTAB	2.43	462.2	0.421	45.7

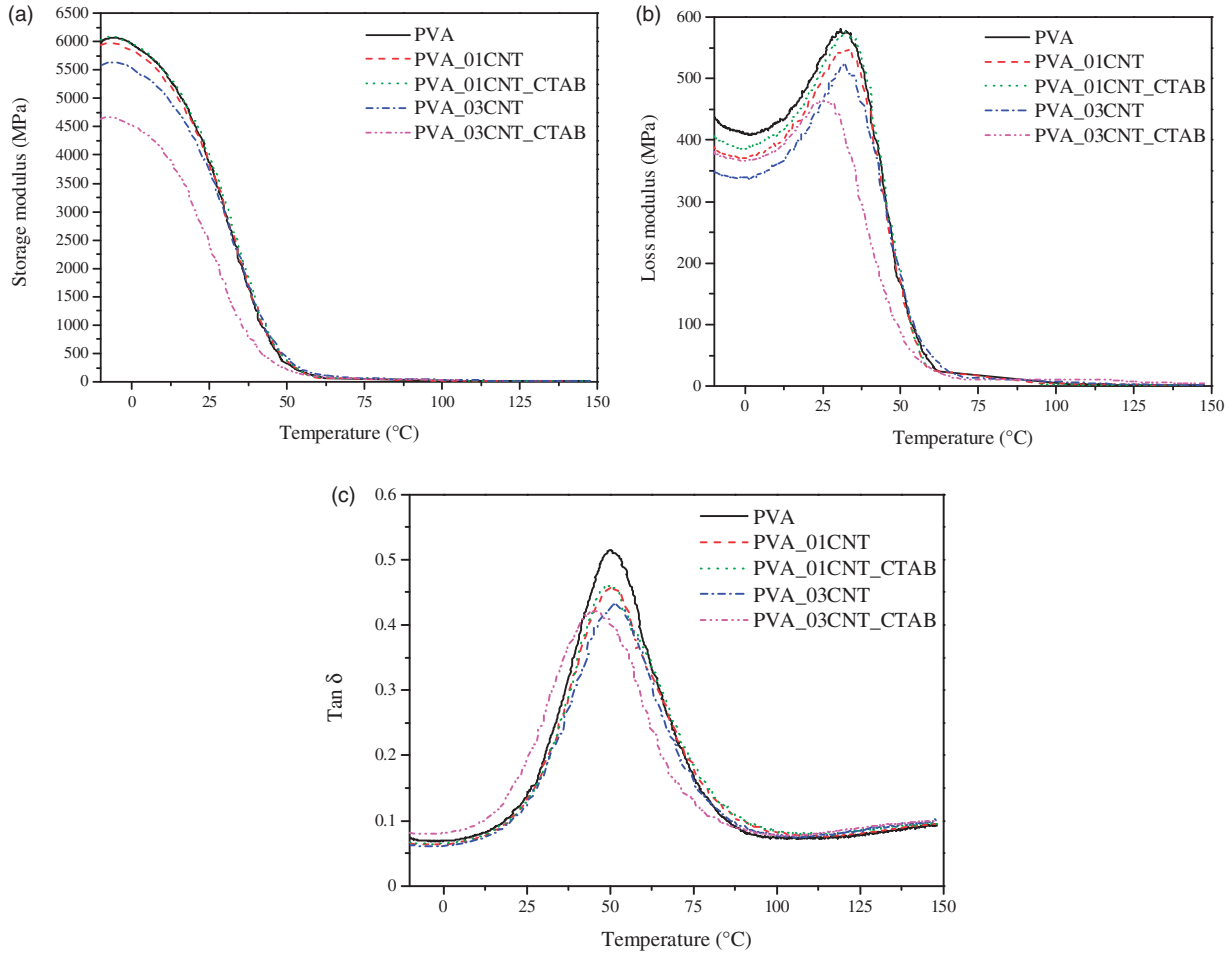

Figure 7. Storage modulus (a), loss modulus (b) and tanδ (c) curves for 3D-printed specimen of PVA and PVA/CNT.

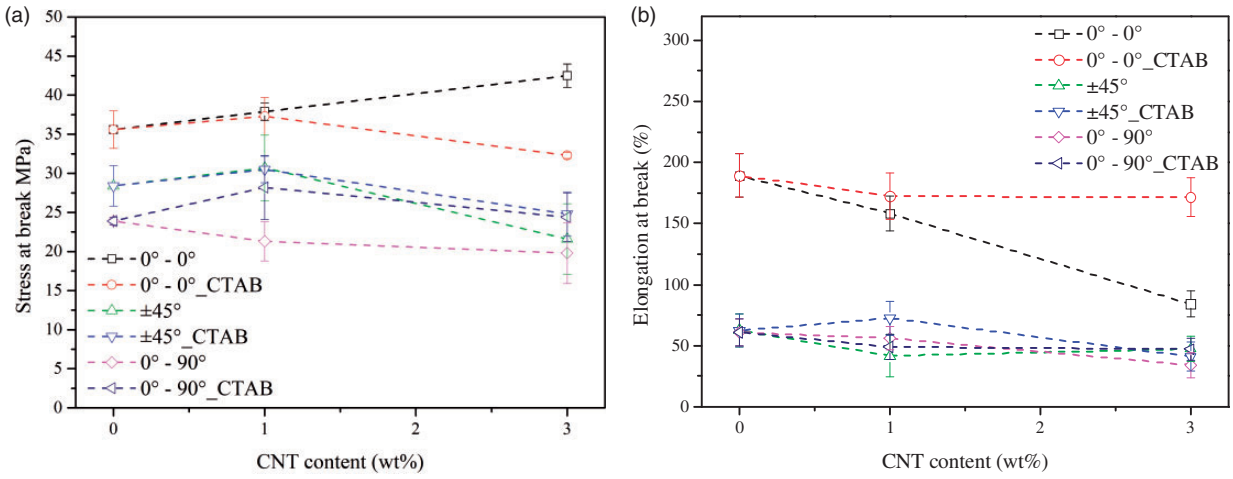

Figure 8. Stress (a) and elongation (b) at break for different kind of printed samples with increasing amount of CNTs. CNT: carbon nanotube.

for the infill orientation of ±45° and 0°/90°. Elongation at break exhibits the same trend with values of 189.2%, 62.5% and 60.9% for infill orientation of 0°/0°, ±45° and 0°/90°, respectively. This behavior could be explained with the orientation of the filaments in the specimen, all in the same direction for the 0°/0° sample, moreover this is the direction where the load was applied during the test, resulting in the maximum resistance. CNTs promote an increase in the stress needed to break the dumbbell specimens and in particular at 1 wt.% and 3 wt.% of nanotubes content, the stress at break for 0°/0° samples reaches values of 37.9 MPa and 42.5 MPa, respectively, that correspond to an increase of 6.5% and 20% with respect to the neat PVA. For the other infill orientation, it is possible to appreciate an increase in the strength at break at 1 wt.% of nanotubes and then a slightly decrease. This effect could be explained with the increase in viscosity that made the printing more difficult, especially along orientations different from 0°/0° where the filaments are not deposited continuously. The presence of the surfactant seems to not influence the properties at break, apart the increase in ductility of the samples printed at 0°/0° direction, where at 3 wt.% of CNTs, the deformation at break is increased counterbalancing a decrease in the stress at break.

In Figure 9, isothermal creep compliance curves are presented for the samples printed at infill angle of ±45° with increasing amount of CNTs. Thermal stability was clearly improved with the introduction of the nanofiller, and creep compliance value measured at 3600 s changed from 41.6 GPa^{-1} of the sample printed with neat PVA to 16.0 GPa^{-1} of the sample with 3 wt.% of CNTs. Although the better dispersion of nanotubes inside the matrix given by the introduction of the surfactant, the creep compliance curves for the samples with CTAB is higher. However, the values are always smaller than the ones for the neat polymer.

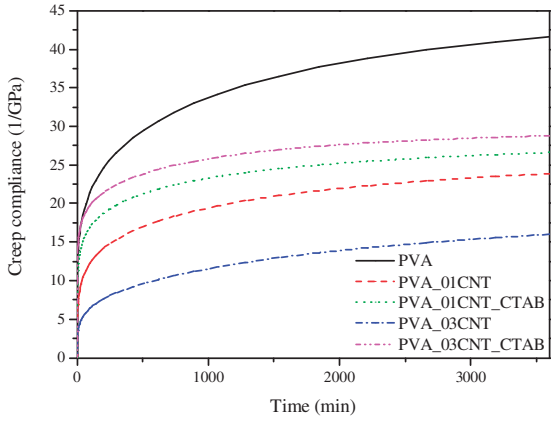

Figure 9. Creep compliance curves for 3D-printed specimen with an infill angle of ±45°.

Electrical resistivity

Electrical resistivity values of the material loaded with increasing amount of CNTs at different manufacturing stages are presented in Figure 10. CNTs improve significantly the electrical conductivity of the bulk material (compression molded) and the resistivity values for filaments are comparable with the ones obtained for plates. A decrease in the electrical properties of the material is observed after the extrusion from the nozzle of the 3D printer and the resistivity remains constant with the increase of CNTs content.

This effect is explained by the aggregation of the CNTs inside the filament extruded by the 3D printer. In fact, Figure 2(a) indicates the presence of CNT-

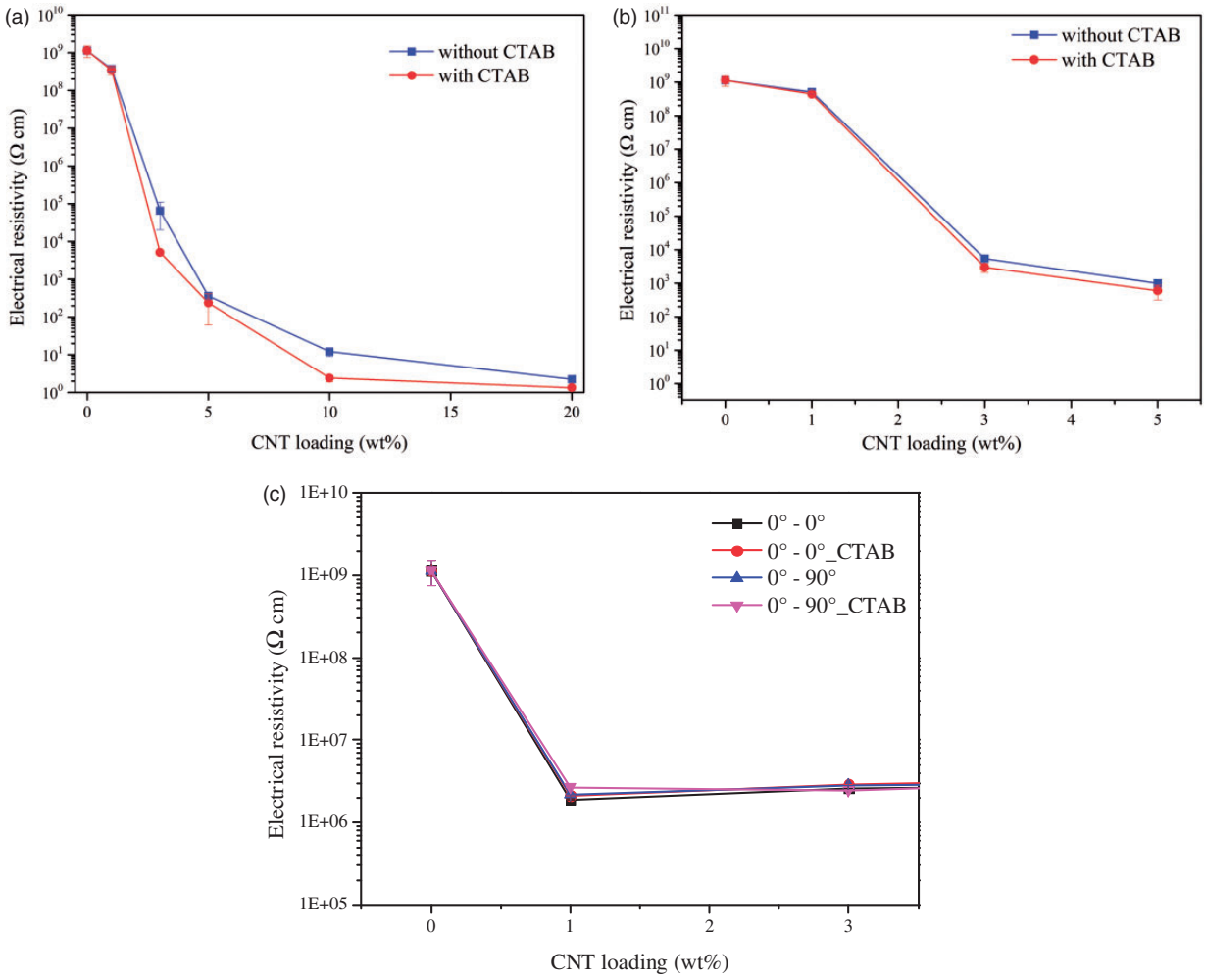

Figure 10. Electrical resistivity for PVA-CNT composites in form of bulk material (a), extruded filament (b) and 3D-printed specimen (c).

Table 4. Electrical resistivity values for 3D-printed samples along two different directions with different amount of CNT and the presence or not of CTAB.

	Electrical resistivity (10^6 Ω cm)
0°–0° orientation	
PVA_CNT01	1.89 ± 0.02
PVA_CNT03	2.59 ± 0.01
PVA_CNT01_CTAB	2.20 ± 0.03
PVA_CNT03_CTAB	2.82 ± 0.06
0°–90° orientation	
PVA_CNT01	2.12 ± 0.03
PVA_CNT03	2.90 ± 0.06
PVA_CNT01_CTAB	2.69 ± 0.01
PVA_CNT03_CTAB	2.47 ± 0.01

enriched zones inside the material. The anisotropy in the electrical properties was evaluated by measuring resistivity at various angles between the deposition direction of the print head and the measuring probes. The results for the 3D-printed samples at different orientation with and without the surfactant are summarized in Table 4. It is possible to notice that the resistivity is always higher in the orthogonal direction in respect to the deposition direction.

Conclusions

In this study, the feasibility of printing 3D composite objects based on PVA containing CNTs, by using a desktop 3D FDM printer, was proved. CNTs were dispersed in the polymer matrix through solution mixing with and without surfactant. Glass transition

temperature of the 3D-printed sample is increased but CTAB has a detrimental effect on it, lowering the glass transition to values comparable with the neat polymer.

The presence of nanotubes causes a slight reduction of strain at break for the 3D-printed samples printed with all the different infill, and concurrently, the stress at break is increased for samples printed with 0°/0° orientation. CNTs were also proven to reduce the creep compliance of the 3D-printed parts so as to improve their stability under long lasting loads. Resistivity of the 3D-printed samples is decreased in respect of the neat polymer but reached the same value for all kind of specimen and it is not influenced by the nanotubes content. Resistivity after 3D printing did not reach the values previously found for filament or for plates. This effect was explained by the formation, during the process of 3D printing, of enriched regions of CNTs inside the filament that were shielded from the outside by the external shell layer of CNTs depauperated material.

Acknowledgements

Mr. Alberto Rossi is gratefully acknowledged for his support to the experimental work.

Declaration of conflicting interests

The author(s) declared no potential conflicts of interest with respect to the research, authorship, and/or publication of this article.

Funding

The author(s) received no financial support for the research, authorship, and/or publication of this article.

References

1. Lee J-Y, An J and Chua CK. Fundamentals and applications of 3D printing for novel materials. *Appl Mater Today* 2017; 7: 120–133.
2. Chiellini E, Corti A, D'Antone S, et al. Biodegradation of poly (vinyl alcohol) based materials. *Prog Polym Sci* 2003; 28: 963–1014.
3. Dorigato A and Pegoretti A. Biodegradable single-polymer composites from polyvinyl alcohol. *Colloid Polym Sci* 2011; 290: 359–370.
4. Andrews R and Weisenberger MC. Carbon nanotube polymer composites. *Curr Opin Solid State Mater Sci* 2004; 8: 31–37.
5. Spitalsky Z, Tasis D, Papagelis K, et al. Carbon nanotube–polymer composites: chemistry, processing, mechanical and electrical properties. *Progr Polym Sci* 2010; 35: 357–401.
6. Xie X, Mai Y and Zhou X. Dispersion and alignment of carbon nanotubes in polymer matrix: a review. *Mater Sci Eng* 2005; 49: 89–112.
7. Chen W, Tao X, Xue P, et al. Enhanced mechanical properties and morphological characterizations of poly (vinyl alcohol)–carbon nanotube composite films. *Appl Surf Sci* 2005; 252: 1404–1409.
8. Coleman JN, Cadek M, Ryan KP, et al. Reinforcement of polymers with carbon nanotubes. The role of an ordered polymer interfacial region. Experiment and modeling. *Polymer* 2006; 47: 8556–8561.
9. Ryan KP, Cadek M, Nicolosi V, et al. Multiwalled carbon nanotube nucleated crystallization and reinforcement in poly (vinyl alcohol) composites. *Synthet Metals* 2006; 156: 332–335.
10. Wang Z, Ciselli P and Peijs T. The extraordinary reinforcing efficiency of single-walled carbon nanotubes in oriented poly(vinyl alcohol) tapes. *Nanotechnology* 2007; 18: 455709.
11. Tong X, Zheng J, Lu Y, et al. Swelling and mechanical behaviors of carbon nanotube/poly(vinyl alcohol) hybrid hydrogels. *Materi Lett* 2007; 61: 1704–1706.
12. Tsai Y-C and Huang J-D. Poly(vinyl alcohol)-assisted dispersion of multiwalled carbon nanotubes in aqueous solution for electroanalysis. *Electrochem Commun* 2006; 8: 956–960.
13. Hou C-H, Liu N-L, Hsu H-L, et al. Development of multi-walled carbon nanotube/poly(vinyl alcohol) composite as electrode for capacitive deionization. *Separat Purif Technol* 2014; 130: 7–14.
14. Castell P, Cano M, Maser WK, et al. Combination of two dispersants as a valuable strategy to prepare improved poly(vinyl alcohol)/carbon nanotube composites. *Compos Sci Technol* 2013; 80: 101–107.
15. Yan WL, Dasari A and Kong LB. Chinese ink-facilitated fabrication of carbon nanotube/polyvinyl alcohol composite sheets with a high nanotube loading. *Compos Part A* 2014; 61: 209–215.
16. Ni W, Wang B, Wang H, et al. Fabrication and properties of carbon nanotube and poly(vinyl alcohol) composites. *J Macromol Sci Part B*. 2006; 45: 659–664.
17. Cox SC, Thornby JA, Gibbons GJ, et al. 3D printing of porous hydroxyapatite scaffolds intended for use in bone tissue engineering applications. *Mater Sci Eng C Mater Biol Appl* 2015; 47: 237–247.
18. Goyanes A, Buanz AB, Basit AW, et al. Fused-filament 3D printing (3DP) for fabrication of tablets. *Int J Pharm* 2014; 476: 88–92.
19. Goyanes A, Chang H, Sedough D, et al. Fabrication of controlled-release budesonide tablets via desktop (FDM) 3D printing. *Int J Pharm* 2015; 496: 414–420.
20. Goole J and Amiqhi K. 3D printing in pharmaceutics: a new tool for designing customized drug delivery systems. *Int J Pharm* 2016; 499: 376–394.
21. Acquah SFA, Leonhardt BE, Nowotarski MS, et al. Carbon nanotubes and graphene as additives in 3D printing. Carbon Nanotubes – Current Progress of their Polymer Composites, Dr Mohamed Berber (Ed.), InTech, 2016; DOI: 10.5772/63419
22. Dorigato A, Moretti V, Dul S, et al. Electrically conductive nanocomposites for fused deposition modelling. *Synthet Metals* 2017; 226: 7–14.

23. Berretta S, Davies R, Shyng YT, et al. Fused deposition modelling of high temperature polymers: exploring CNT PEEK composites. *Polym Test* 2017; 63: 251–262.
24. Kim K, Park J, Suh J-h, et al. 3D printing of multiaxial force sensors using carbon nanotube (CNT)/thermoplastic polyurethane (TPU) filaments. *Sensors Actuat A* 2017; 263: 493–500.
25. Christ JF, Aliheidari N, Ameli A, et al. 3D printed highly elastic strain sensors of multiwalled carbon nanotube/thermoplastic polyurethane nanocomposites. *Mater Des* 2017; 131: 394–401.
26. Gnanasekaran K, Heijmans T, van Bennekom S, et al. 3D printing of CNT- and graphene-based conductive polymer nanocomposites by fused deposition modeling. *Appl Mater Today* 2017; 9: 21–28.
27. Thomas D, Zhuravlev E, Wurm A, et al. Fundamental thermal properties of polyvinyl alcohol by fast scannig calorimetry. *Polymer* 2018; 137: 145–155.
28. Thomas PS, Guerbois JP, Russell GF, et al. The thermal degradation of poly(vinyl alcohol). *J Therm Anal Calorimetry* 2001; 64: 501–508.